Bias Scheme Reducing Transient Currents and Speeding up Read Operations for 3-D Cross Point PCM

Yu Lei, Meng Liu, Houpeng Chen, Xi Li, Qian Wang and Zhitang Song

***Abstract*—3-D cross point phase change memory (PCM) is a promising emerging nonvolatile memory in changing the current memory-storage hierarchy. However, dynamic performances of 3-D cross point PCM are limited and the role of bias scheme is unknown. Previous studies on bias schemes for planar memories use static analyses to assess static array performances. Here we use dynamic analyses to assess dynamic chip performances with device parameters, bias schemes, arrays and circuits. A high peak transient read current is found to result in a long read access time. Three factors which contribute to the high peak read current are analyzed. Among them, the high voltage variation of half-selected cells on the bit line is optimized by scheme design. The proposed 2*V*/3 bias scheme and a single-reference parasitic-matching sensing circuit are utilized in a 64Mbit 3-D cross point PCM. The maximum value of read current is 160.27μA and reduced by 41.7% compared to the conventional *V*/2 scheme. And the sensing time is 30.89ns which is reduced by 22.5%. The chip shows zero read error in Monte Carlo simulations. Designing bias schemes through dynamic analyses paves the way for the development of high-performance 3-D PCM technology to boost the working efficiency of computing systems.**

***Index Terms*—3-D integrated circuits, phase change memory (PCM), cross point, bias scheme, dynamic analysis.**

I. Introduction

MONOLITHIC three-dimensional integrated circuits (3-D ICs) are actively under research and development in order to keep pace with Moore's law doubling the number of transistors every 18 months [1]-[4]. Among them, 3-D cross point phase change memory (PCM) promises to replace NAND Flash and fundamentally changes the memory-storage hierarchy because of its combination of high performance, high density and nonvolatility [5]-[8]. However, the chip performance is now limited by parasitic elements, sneak currents and vertical integration, which can be enhanced by the optimization of bias schemes [9]-[12].

3-D cross point memory uses stacked cross point arrays where metal lines are orthogonally crossing one over another, and a memory cell is formed at each intersection[13]-[16]. Three common read schemes in a planar crossbar or cross point array-the ground, V/2, and V/3 schemes-have been extensively studied [17]-[21]. In 3-D cross point array architecture, the introduction of the ground scheme will select all the up and down layer memory cells on the selected word line (WL). Therefore partial bias schemes are favorable as they support a single bit read in a subarray [22]-[24]. The V/3 bias scheme has much higher power consumption than the V/2 bias scheme [16], [25]-[28], which may not be acceptable in 3-D memory. Selectors which are capable of bidirectional operation, such as ovonic threshold switch (OTS) and mixed-ionic-electronic-conduction (MIEC), can be utilized in 3-D cross point PCM [29]-[33]. V/2 bias scheme is favorable in this memory because of supporting a single bit read, low sneak currents and good compatibility with bidirectional selector [16], [34].

Previous studies on bias schemes use static analyses to assess array performance (power consumption, writing voltage margin and sensing margin) with device parameters and array design details. However, dynamic simulations for assessing chip performance (dynamic power consumption, read access time and read errors) with device parameters, bias schemes, arrays and circuits are rarely reported.

Lei *et al*. [34] proposed a single-reference parasitic-matching (SRPM) sensing circuit for 3-D cross point PCM with considerations of factors that affect the read operation. Different from conventional read reference currents [15], [24], its reference current changes and shares a similar curve with the read current.

In this article, we introduce dynamic simulations into state-of-the-art and conventional sensing circuits to analyze limitations of chip performances and bias schemes. Chip performances between combinations of different sensing circuits and bias schemes are also compared. It is shown that

This paragraph of the first footnote will contain the date on which you submitted your paper for review. This work was supported in part by the General Research Projects of State Key Laboratory of Functional Materials for Informatics under Grant 1199003YXM, by the National Key Research and Development Program of China under Grants 2018YFB0407500, 2017YFA0206101, 2017YFA0206104, 2017YFB0701703 and SQ2017YFGX020134, by the National Natural Science Foundation of China under Grants 61874129, 61874178 and 61622408, and by the Science and Technology Council of Shanghai under Grants 18DZ2272800 and 17DZ2291300.

Y. Lei is with the State Key Laboratory of Functional Materials for Informatics, Shanghai Institute of Micro-System and Information Technology, Chinese Academy of Sciences, Shanghai 200050, China, and also with Shanghai Nanotechnology Promotion Center, Shanghai 200237, China, (e-mail: leiyuthuniverse@gmail.com).

M. Liu, H. Chen, X. Li, Q. Wang and Z. Song are with the State Key Laboratory of Functional Materials for Informatics, Shanghai Institute of Micro-System and Information Technology, Chinese Academy of Sciences, Shanghai 200050, China.

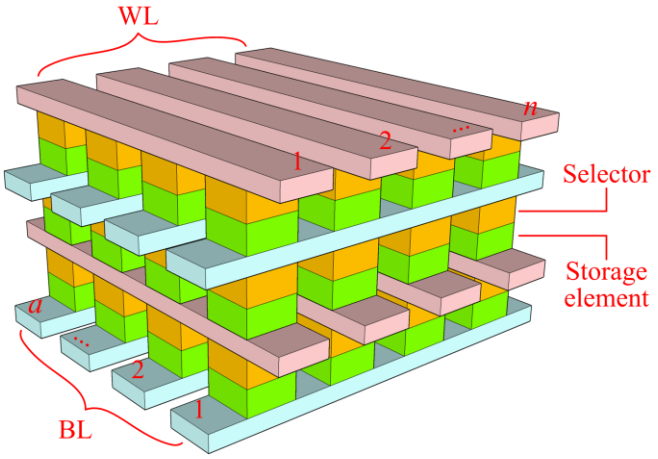

Fig. 1. Schematic of the 3-D cross point PCM array.

the high voltage variation of half-selected cells on the selected bit line (BL) and the relatively high threshold voltage of selector are main causes of speed limits. Therefore, a 2*V*/3 bias scheme is proposed here to enhance the read performance.

The remainder of this paper is organized as follows. Section II introduces the array architecture, conventional bias scheme and the array core circuit. Section III analyzes limitations of chip performance and the role of bias scheme. Section IV introduces the proposed 2*V*/3 bias scheme. Section V presents evaluation results and discussions. Finally, Section VI concludes the paper.

II. Building 3-D Cross Point PCM

Fig. 1 shows the schematic of the 3-D cross point PCM array. In the memory cell, the selector and the storage element are connected in series between the WL and the BL. In each array, the number of memory layers is twice the number of BLs; there are *n* WLs connected to one BL in each layer of WL, *a* BLs connected to one WL, *m* BLs connected to one local bit line (RBL_L), *c* RBL_Ls connected to one sense amplifier (SA) through a global bit line (RBL_G), *b* SAs connected to one read reference circuit.

Fig. 2 illustrates the *V*/2 bias scheme. The selected BL and WL are biased to *V* and 0, respectively. The unselected BL and WL are biased to *V*/2. *V* is the BL read voltage. I_{read} is the source current of RTG_L. I_{cell} is the cell read current. I_{read1} is the source current of NM_{A1}. I_{charge} is the charge current of the half-selected cell. I_{sneak} is the cell sneak current. V_C is the voltage of the memory cell. In the read operation, cells in the subarray can be divided into four groups. Each group is classified depending on the decoding scheme of WLs and BLs as shown in Table I.

BL operates two layers of memory cells. The array core circuit is designed accordingly, as shown in Fig.3. The circuit comprises a deselect BL voltage source (DESBL) and a deselect WL voltage source (DESWL). Voltages supplied by DESBL and DESWL voltage sources are designed according to the bias scheme. BL is connected to the programming bit line (PBL) and the read bit line (RBL) through the programming transmission gate (PTG) and the read transmission gate (RTG), respectively. EN signal controls read and write operations.

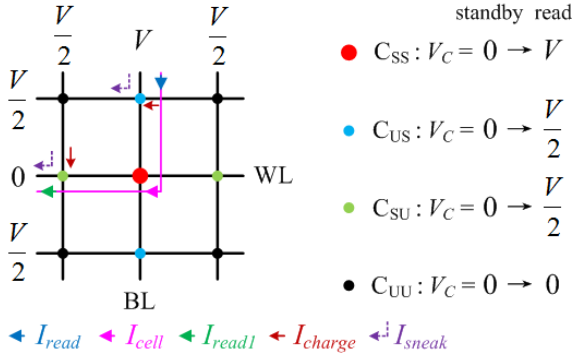

Fig. 2. *V*/2 bias scheme and voltage variations of cells in standby and read phases.

TABLE I
CELLS DIVIDED INTO FOUR GROUPS

Symbol	WL	BL
C_{SS}	Selected	Selected
C_{US}	Unselected	Selected
C_{SU}	Selected	Unselected
C_{UU}	Unselected	Unselected

WL_1<*n*-1:0> and WL_2<*n*-1:0> are up and down layer WLs which are connected to the same BL. Totally, 2*n* cells are connected to one BL in each array core circuit. Y_G and Y_L are global and local select buses, respectively. They control corresponding gates and BLs.

III. Conventional Bias Scheme and Analysis

The 64Mbit 3-D cross point PCM has two-stacked-layers of memory cells, two layers of WL and one layer of BL. Each memory layer is divided into 4 banks. Each bank comprises 8 tiles of sub-banks (1024 rows × 1024 columns). In the array, *n*=1024, *a*=1024, *m*=16, *c*=16, *b*=8. Every 512Kbit (1024 rows × 1 column × 2 layers × 16 LTGs × 16GTGs) share an SA. Periphery circuits are designed in the SMIC 40nm CMOS process. The supply voltage is 2.5V. The chip utilizes the *V*/2 bias scheme and the SRPM sensing circuit [34].

Parameters used in the simulation are listed in Table II, based on [16], [29], [30], [35]-[38]. R_{PCM} is the PCM resistance. Compared to the previous research [34], the switching speed of selector and the line resistance are considered. The selector compact model in this paper is also based on [29], [30], [35], [36], [38]. The model of PCM is based on [39].

Fig. 4 and Fig. 5 are simulation results of the chip when RTG_L<0>, RTG_G<0>, BL<0> and WL_1<0> are selected. R_{PCM} are 10KΩ (set) and 2MΩ (reset), respectively. The read current is as small as 5.49μA. R_{ref} is 250KΩ. I_{refnew} is set between I_{read} (@ worst set R_{PCM}) and I_{read} (@ worst reset R_{PCM}). The sensing time is 39.66ns which is determined by the set speed. The peak value of I_{read} and I_{ref} are 274.91μA and 274.96μA, respectively. The sensing time is 39.86ns when RTG_L<15>, RTG_G<15>, BL<1023> and WL_1<1023> are selected.

In the read operation, SA has to charge parasitic capacitors in the array, which enlarges the read current and delays the read operation. In planar PCM, most of parasitic elements are planar

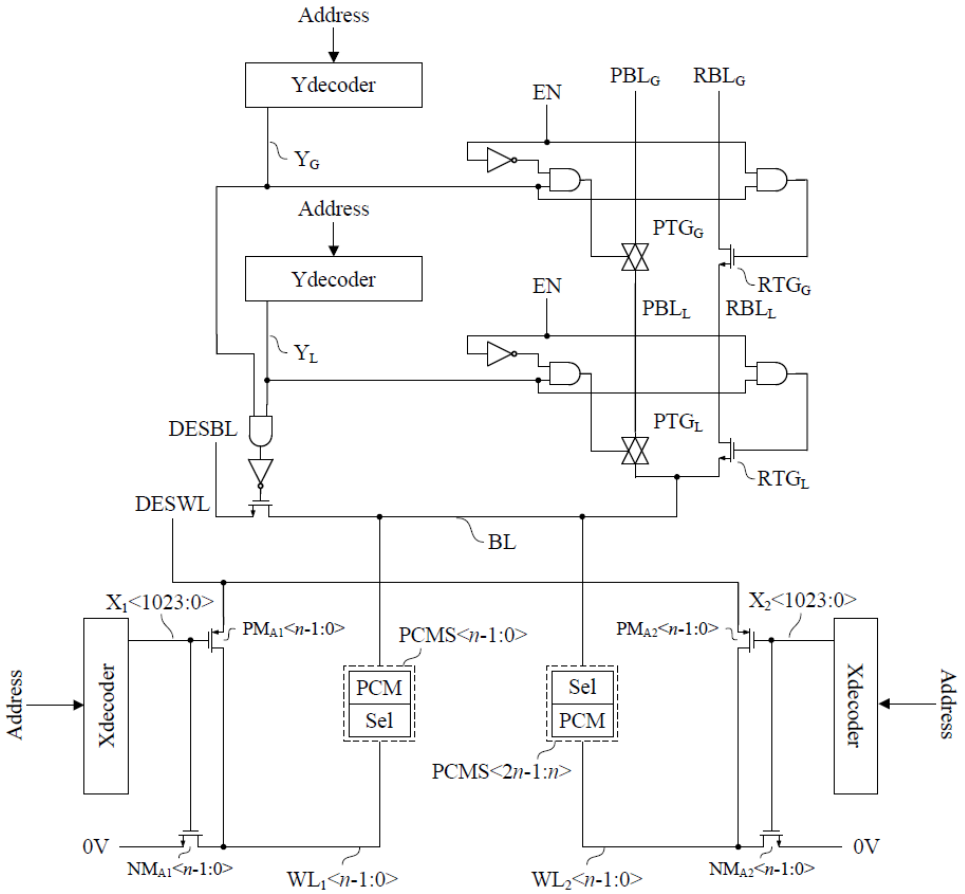

Fig. 3. Array core design. PCMS: PCM+selector (Sel).

TABLE II
SIMULATION PARAMETERS

Symbol	Parameter	Value
V_{sth}	Selector threshold voltage	1.5V
-	Selector On/off ratio	10^7
-	Selector parasitic capacitance	1fF
-	Selector switching speed	10ns
-	PCM parasitic capacitance	500aF
-	PCM set resistance (regular)	10KΩ
-	PCM set resistance (worst)	100kΩ
-	PCM reset resistance (regular)	2MΩ
-	PCM reset resistance (worst)	1MΩ
-	Line interconnect resistance (Cu)[a]	1Ω
V ($@R_{PCM}$)	BL voltage in the read operation	1.65V (2MΩ); 1.56V (10KΩ)
V / 2	DESBL / DESWL voltage	0.82V
2 V / 3	DESBL / DESWL voltage	1.1V
I_{sneak1}	Cell sneak current ($@V_{read}$ / 2, R_{PCM}=10KΩ)	10pA
I_{sneak2}	Cell sneak current ($@V_{read}$ / 3, R_{PCM}=10KΩ)	0.6pA
I_{sneak3}	Cell sneak current ($@$ 2 V_{read} / 3, R_{PCM}=10KΩ)	2nA

[a] Between adjacent cells.

parasitic elements. But in 3D PCM, vertical parasitic elements will also delay the read operation. In the SRPM sensing scheme, factors that affect the read operation in 3-D cross point PCM are all considered and I_{refnew} shares a similar curve with I_{cell}.

However, a high peak I_{read} still exists in the SRPM scheme. At

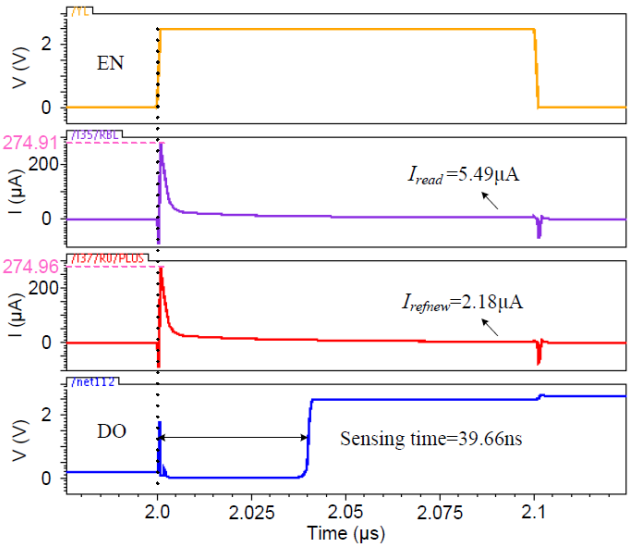

Fig. 4. Simulation results of the conventional bias scheme (set).

the beginning of the read operation, I_{read} rises to their maximum currents, then drops exponentially [9], [37]. It is costly for I_{read} dropping from the maximum value to the stable value. A high peak I_{read} increases the read access time and the dynamic power consumption.

Three factors contribute to a high peak I_{read} for 3-D cross point memory:

1) Parasitic capacitors in the array [34]. As the capacity of memory becomes larger, the number of parasitic capacitors in

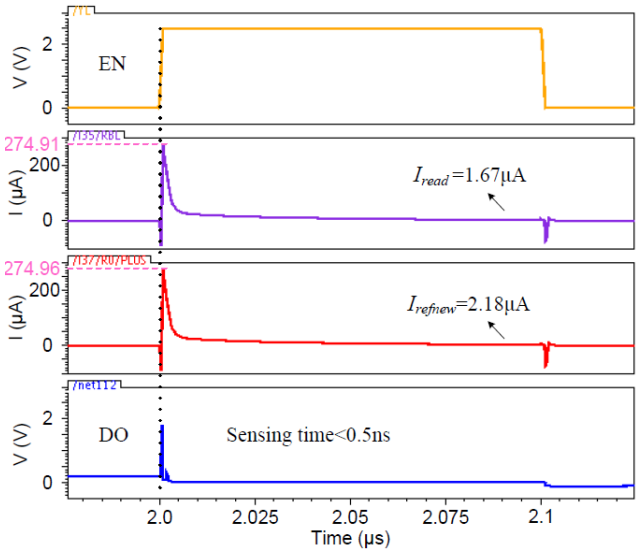

Fig. 5. Simulation results of the conventional bias scheme (reset).

the array becomes larger. For 64Mbit 3-D cross point PCM chip, there are 2048 cells connected to the BL.

2) High threshold voltage of the selector. V should be higher than selector threshold voltage V_{sth}, or between Vt_{set} and Vt_{reset} (Kau *et al.*'s definition [29]) to conduct a read operation. But V_{sth} of emerging selectors is larger than that of diodes and V_{ds} of transistors [29], [30], [35], [36].

3) High voltage variation of half-selected cells on the BL. It is not V_C but the voltage variation of the cell that contributes to a high peak read current. The voltage variations of cells in the $V/2$ bias scheme are shown in Fig. 2. The voltage variation of C_{SS} between the standby and read phases is V. There is only one selected cell, and its influence on a high peak I_{read} is small. The voltage variations of C_{US} and C_{SU} are $V/2$. Due to their opposite I_{charge} directions, C_{US} has a much bigger impact on the high peak I_{read} than C_{SU} [22], [34]. The voltage variation of C_{UU} is 0. In general, the high voltage variation of C_{US} contributes most among four cell groups.

These three factors all lead to an extra charging process in the read operation. First two factors can be optimized by circuit and device designs. The last one can be optimized by scheme design.

IV. Proposed 2V/3 Bias Scheme

The main aim of the proposed read bias scheme is to reduce the high voltage variation of C_{US} without severe sacrificing other performances of the chip. The proposed $2V/3$ bias scheme is illustrated in Fig.6. The selected BL and WL are biased to V and 0, respectively. The unselected BL and WL are biased to $2V/3$. The voltage variation of C_{SS} and C_{UU} are still V and 0, respectively. The voltage variations of C_{US} and C_{SU} are $V/3$ and $2V/3$, respectively.

For C_{US}, I_{charge} comes from the selected BL, which weakens I_{read}. The voltage variation of the $2V/3$ scheme is decreased from $V/2$ to $V/3$, comparing to that of the $V/2$ scheme. For C_{SU}, I_{charge} comes from the unselected BL, which would not affect the transient value of I_{read} directly. Despite an increase in voltage variation, I_{charge} of C_{SU} still has a little impact on a high

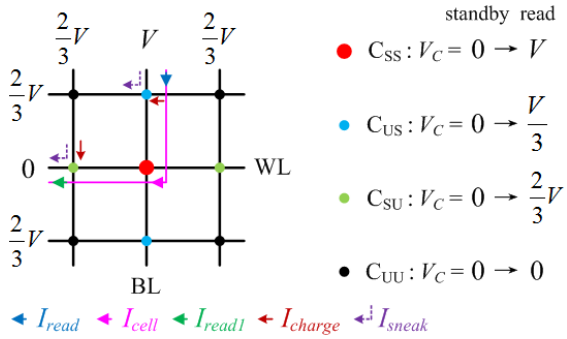

Fig. 6. $2V/3$ bias scheme and voltage variations of cells in standby and read phases.

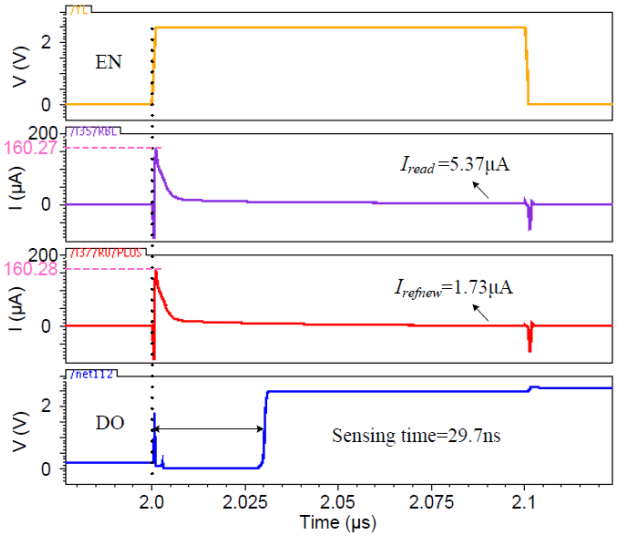

Fig. 7. Simulation results of the proposed bias scheme (set).

peak I_{read}.

The proposed scheme also brings changes in the amount of I_{sneak} for cell groups. I_{sneak} of C_{US} decreases, which is good for the reduction of read errors. Meanwhile, I_{sneak} of C_{SU} increases. As it comes from the unselected BL to the selected BL, I_{sneak} of C_{SU} would not affect the stable value of I_{read} directly and has a little impact on it.

Compared to the conventional bias scheme, the proposed scheme will lower the maximum value of I_{read} (or dynamic power consumption) and read errors. As the result of a reduced peak value of I_{read}, a short read access time can be measured. In addition, C_{UU} has no sneak current, avoiding full-array-current-sneaking. Therefore, the $2V/3$ bias scheme has much lower power consumption than the $V/3$ bias scheme.

In the proposed scheme, $2V/3$ should be lower than V_{sth} for a low sneak current of two-third selected cells. Moreover, DESBL and DESWL voltages can be other than $2V/3$ as long as they are higher than $V/2$. For example, $3V/5$, $4V/5$, etc. The DESBL and DESWL voltages should also be lower than V_{sth}. All these bias schemes have similar advantages as $2V/3$ bias scheme.

V. Performance Evaluation

We then utilize the $2V/3$ bias scheme and the SRPM sensing circuit in a 64Mbit 3-D cross point PCM. Simulation

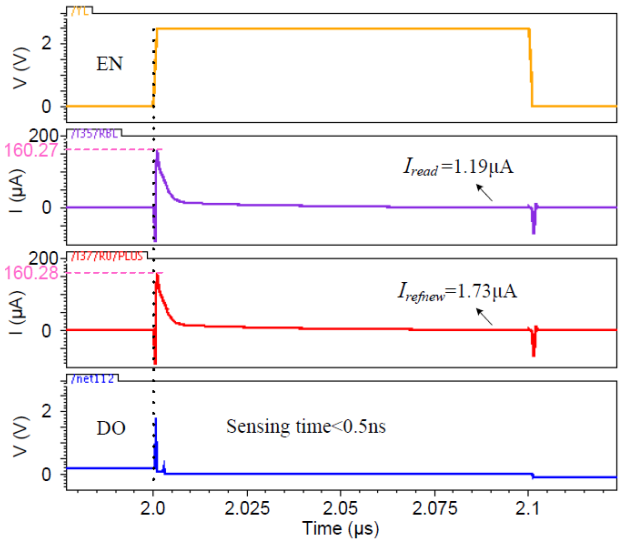

Fig. 8. Simulation results of the proposed bias scheme (reset).

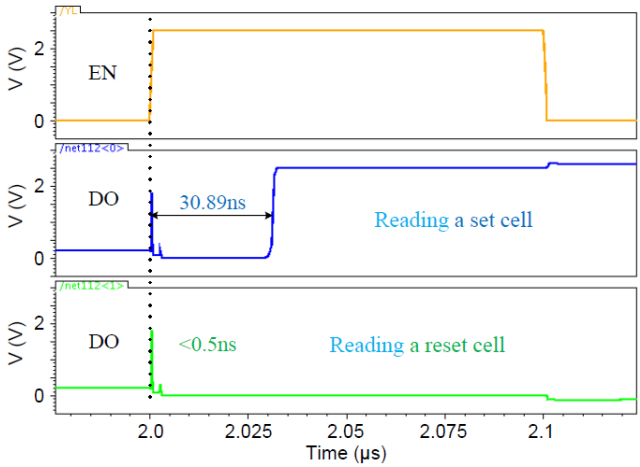

Fig. 9. Simulation results of 64Mbit 3-D cross point PCM when RTG_L<15>, RTG_G<15>, BL<1023> and WL_1<1023>are selected.

parameters of the 2*V*/3 bias scheme are listed in Table II.

Fig. 7 and Fig. 8 are simulation results of the proposed chip when RTG_L<0>, RTG_G<0>, BL<0> and WL_1<0> are selected. The peak value of I_{read} and I_{ref} are 160.27μA and 160.28μA which are reduced by 114.64μA and 114.68μA, respectively. The sensing time is 29.7ns. The read and reference currents are all reduced (set: 5.49μA to 5.37μA, reference: 2.18μA to 1.73μA, reset: 1.67μA to 1.19μA). Compared to the conventional scheme, the sensing time, maximum and stable values of I_{read} are greatly decreased, which is also consistent with our theoretical analysis in Section IV.

Simulation results of the proposed chip when RTG_L<15>, RTG_G<15>, BL<1023> and WL_1<1023> are selected are shown in Fig.9. The sensing time is 30.89ns which is reduced by 22.5% compared to the conventional *V*/2 scheme. The sensing time of the proposed chip differs due to the resistance of the long BL and WL.

Fig. 10 presents simulation results for four combinations of sensing circuits and bias schemes. The results include the sensing time of the regular simulation, the worst case sensing time of the Monte Carlo simulation and read errors. The read performance is evaluated under both the regular and the worst R_{PCM}. In simulations, RTG_L<15>, RTG_G<15>, BL<1023> and WL_1<1023> are selected. The sensing time of the SRPM sensing circuit is reduced by 5.68ns under the worst R_{PCM} with the proposed bias scheme. That of the conventional sensing circuit is reduced by 16.34ns and 16.86ns under the regular and the worst R_{PCM}, respectively. The 2*V*/3 bias scheme speeds up the read operation for both SRPM and conventional sensing circuits.

Monte Carlo simulations are performed using the industry compatible SMIC 40-nm model parameters. The simulation is conducted with the whole array and the periphery circuit. Accomplished in process & mismatch analysis, six times standard deviation (6σ) is used as variances of parameters and mismatches of MOSs and resistors. In each simulation, 4000 trials are run. The worst case sensing time of the SRPM sensing circuit is reduced by 50.04ns and 78.23ns under the regular and the worst R_{PCM}, respectively, with the 2*V*/3 bias scheme. That of the conventional sensing circuit is reduced by 28.64ns and 37.9ns under the regular and the worst R_{PCM}, respectively. Read errors are reduced for both SRPM (by 100%) and conventional (by 28.98%) sensing circuits. In particular, results of the SRPM circuit and the 2*V*/3 scheme show zero read error under the regular and the worst R_{PCM}. Based on the above simulation results, the 2*V*/3 bias scheme is verified to be robust to process variations and have superiority over the conventional *V*/2 bias scheme.

VI. Conclusion

We have reported the design of a 2*V*/3 bias scheme for 3-D cross point PCM. Better dynamic performances have been achieved, such as shorter read access time, lower dynamic power consumption and less read errors. The design uses dynamic simulations to assess dynamic chip performances with device parameters, bias schemes, arrays and circuits, in contrast to traditional static analyses. The simulations show a high peak read current at the beginning of the read operation, which increases the read access time. Three factors which contribute to this high current are analyzed, and a read bias scheme for reducing the high voltage variation of half-selected cells on the BL is proposed. The 2*V*/3 bias scheme exhibits lower maximum and stable values of read current and consequently a lower sensing time for both SRPM and conventional sensing circuits. The scheme proves to have fast read access time even for the edge of the array. Chip performances of four combinations of sensing circuits and bias schemes have been compared, and the 2*V*/3 bias scheme is verified to be robust to process variations and have superiority over the conventional *V*/2 bias scheme. The dynamic analyses prove to be powerful in the optimization of bias scheme and the improvement of chip's dynamic performances. The next steps will be to utilize dynamic analyses of bias scheme to planar and other 3-D emerging memories.

Acknowledgment

We thank G. Liu and S. Zhang for useful discussions and Y. Xu, E. Deng and Y. Xia for reviewing the manuscript.

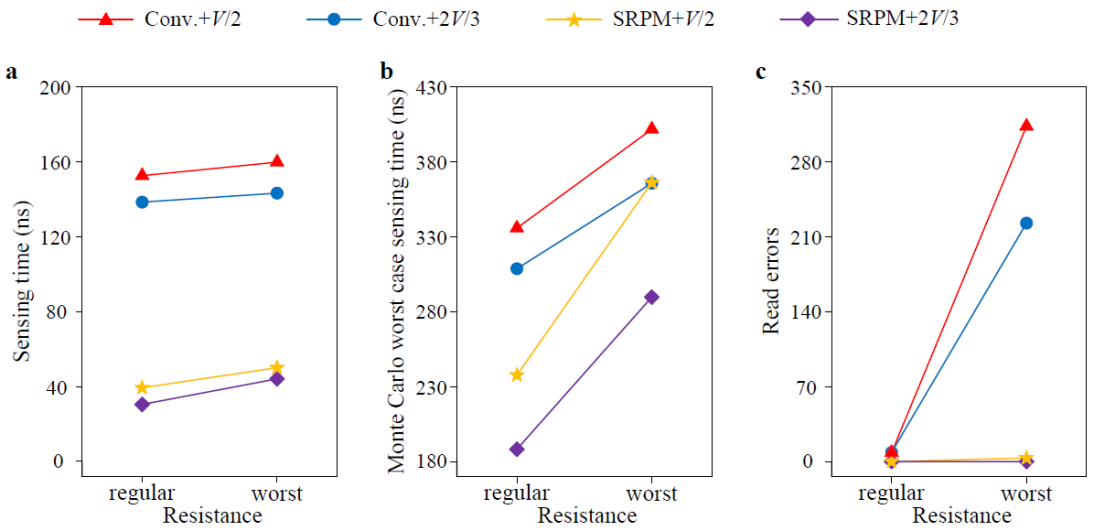

Fig. 10. Performance comparison between four combinations of sensing circuits and bias schemes. (a) Sensing time of the regular simulation. (b) Worst case sensing time of Monte Carlo simulations. (c) Read errors in each Monte Carlo simulation. Conv.: conventional circuit.

REFERENCES

[1] R. Micheloni, S. Aritome and L. Crippa, "Array Architectures for 3-D NAND Flash Memories," in *Proceedings of the IEEE*, vol. 105, no. 9, pp. 1634-1649, Sept. 2017.

[2] S. Srinivasa, X. Li, M. F. Chang, J. Sampson, S. K. Gupta and V. Narayanan, "Compact 3-D-SRAM Memory With Concurrent Row and Column Data Access Capability Using Sequential Monolithic 3-D Integration," in *IEEE Transactions on Very Large Scale Integration (VLSI) Systems*, vol. 26, no. 4, pp. 671-683, April 2018.

[3] Yoon, Jae Woong, et al. "Nanophotonic identification of defects buried in three-dimensional NAND flash memory devices." *Nature Electronics* 1.1 (2018): 60.

[4] Z. Zhang, Y. Y. Liauw, C. Chen and S. S. Wong, "Monolithic 3-D FPGAs," in *Proceedings of the IEEE*, vol. 103, no. 7, pp. 1197-1210, July 2015.

[5] Intel and Micron Produce Breakthrough Memory Technology. (2015). [Online]. Available: http://newsroom.intel.com/community/intel_newsroom/blog/2015/07/28/intel-and-micron-produce-breakthrough-memory-technology

[6] F. T. Hady, A. Foong, B. Veal and D. Williams, "Platform Storage Performance With 3D XPoint Technology," in *Proceedings of the IEEE*, vol. 105, no. 9, pp. 1822-1833, Sept. 2017.

[7] G. W. Burr *et al.*, "Recent Progress in Phase-Change Memory Technology," in *IEEE Journal on Emerging and Selected Topics in Circuits and Systems*, vol. 6, no. 2, pp. 146-162, June 2016.

[8] S. Yu and P. Y. Chen, "Emerging Memory Technologies: Recent Trends and Prospects," in *IEEE Solid-State Circuits Magazine*, vol. 8, no. 2, pp. 43-56, Spring 2016.

[9] Y. Lei *et al.*, "Set/reset reference and parasitic matching scheme to speed up PCM read operation," in *Electronics Letters*, vol. 53, no. 3, pp. 144-146, 2 2 2017.

[10] H. Lim, W. Sun and H. Shin, "ReRAM Crossbar Array: Reduction of Access Time by Reducing the Parasitic Capacitance of the Selector Device," in *IEEE Transactions on Electron Devices*, vol. 63, no. 2, pp. 873-876, Feb. 2016.

[11] Integrated Circuit Design of 3-D Cross Point Phase Change Memory: A Single-Reference Parasitic-Matching Sensing Circuit for 3-D Cross Point PCM. (2018). [Online]. Available: https://player.vimeo.com/video/272605360

[12] R. Micheloni (Ed.). 3D Flash memories, *Springer Netherlands*, 2016.

[13] Y. Deng *et al.*, "Design and optimization methodology for 3D RRAM arrays," *2013 IEEE International Electron Devices Meeting*, Washington, DC, 2013, pp. 25.7.1-25.7.4.

[14] I. G. Baek *et al.*, "Realization of vertical resistive memory (VRRAM) using cost effective 3D process," in *Proc. IEEE Int. Electron Devices Meeting (IEDM)*, Washington, DC, 2011, pp. 31.8.1-31.8.4.

[15] T. y. Liu *et al.*, "A 130.7-mm^2 2-Layer 32-Gb ReRAM Memory Device in 24-nm Technology," *IEEE J. Solid-State Circuits*, vol. 49, no. 1, pp. 140-153, Jan. 2014.

[16] M. Mao, S. Yu and C. Chakrabarti, "Design and Analysis of Energy-Efficient and Reliable 3-D ReRAM Cross-Point Array System," in *IEEE Transactions on Very Large Scale Integration (VLSI) Systems*, vol. 26, no. 7, pp. 1290-1300, July 2018.

[17] S. Yu, et al. "Read/write schemes analysis for novel complementary resistive switches in passive crossbar memory arrays." *Nanotechnology* 21.46 (2010): 465202.

[18] A. Ciprut and E. G. Friedman, "Hybrid Write Bias Scheme for Non-Volatile Resistive Crossbar Arrays," *2018 IEEE International Symposium on Circuits and Systems (ISCAS)*, Florence, Italy, 2018, pp. 1-5.

[19] C. Lo, T. Hou, M. Chen and J. Huang, "Dependence of Read Margin on Pull-Up Schemes in High-Density One Selector − One Resistor Crossbar Array," in *IEEE Transactions on Electron Devices*, vol. 60, no. 1, pp. 420-426, Jan. 2013.

[20] L. Song, et al. "An efficient method for evaluating RRAM crossbar array performance." *Solid-State Electronics* 120 (2016): 32-40.

[21] S. Choi, W. Sun, H. Lim and H. Shin, "An analysis of the read margin and power consumption of crossbar ReRAM arrays," *TENCON 2015 - 2015 IEEE Region 10 Conference*, Macao, 2015, pp. 1-3.

[22] Y. Lei *et al.*, "A Changing-Reference Parasitic-Matching Sensing Circuit for 3-D Vertical RRAM," in *IEEE Transactions on Very Large Scale Integration (VLSI) Systems*, vol. 26, no. 7, pp. 1268-1276, July 2018.

[23] A. Chen, "Analysis of Partial Bias Schemes for the Writing of Crossbar Memory Arrays," in *IEEE Transactions on Electron Devices*, vol. 62, no. 9, pp. 2845-2849, Sept. 2015.

[24] C. J. Chevallier *et al.*, "A 0.13μm 64Mb multi-layered conductive metal-oxide memory," in *Proc. IEEE Int. Solid-State Circuits Conf. (ISSCC)*, San Francisco, CA, 2010, pp. 260-261.

[25] Sun, Wookyung, Sujin Choi, and Hyungsoon Shin. "A new bias scheme for a low power consumption ReRAM crossbar array." *Semiconductor Science and Technology* 31.8 (2016): 085009.

[26] A. Chen, "A Comprehensive Crossbar Array Model With Solutions for Line Resistance and Nonlinear Device Characteristics," in *IEEE Transactions on Electron Devices*, vol. 60, no. 4, pp. 1318-1326, April 2013.

[27] Kim, Sungho, Hee-Dong Kim, and Sung-Jin Choi. "Numerical study of read scheme in one-selector one-resistor crossbar array." *Solid-State Electronics* 114 (2015): 80-86.

[28] A. Chen, "Comprehensive methodology for the design and assessment of crossbar memory array with nonlinear and asymmetric selector devices," *2013 IEEE International Electron Devices Meeting*, Washington, DC, 2013, pp. 30.3.1-30.3.4.

[29] D. Kau *et al.*, "A stackable cross point Phase Change Memory," in *Proc. IEEE Int. Electron Devices Meeting (IEDM)*, Baltimore, MD, 2009, pp. 1-4.

[30] G. W. Burr *et al*., “Access devices for 3D crosspoint memory,” *J. Vac. Sci. Technol. B*, 2014, 32(4):040802 - 040802-23.
[31] P. Narayanan *et al*., "Exploring the Design Space for Crossbar Arrays Built With Mixed-Ionic-Electronic-Conduction (MIEC) Access Devices," in *IEEE Journal of the Electron Devices Society*, vol. 3, no. 5, pp. 423-434, Sept. 2015.
[32] G. W. Burr *et al*., "Recovery dynamics and fast (sub-50ns) read operation with Access Devices for 3D crosspoint memory based on mixed-ionic-electronic-conduction (MIEC)," *2013 Symposium on VLSI Technology*, Kyoto, 2013, pp. T66-T67.
[33] G. W. Burr *et al*., "Large-scale (512kbit) integration of multilayer-ready access-devices based on mixed-ionic-electronic-conduction (MIEC) at 100% yield," *2012 Symposium on VLSI Technology (VLSIT)*, Honolulu, HI, 2012, pp. 41-42.
[34] Y. Lei *et al*., "A Single-Reference Parasitic-Matching Sensing Circuit for 3-D Cross Point PCM," in *IEEE Transactions on Circuits and Systems II: Express Briefs*, vol. 65, no. 4, pp. 486-490, April 2018.
[35] H. Yang *et al*., "Novel selector for high density non-volatile memory with ultra-low holding voltage and 10^7 on/off ratio," in *Proc. Symp. IEEE VLSI Technol.*, 2015, pp. T130-T131.
[36] K. Gopalakrishnan *et al*., "Highly-scalable novel access device based on Mixed Ionic Electronic conduction (MIEC) materials for high density phase change memory (PCM) arrays," *2010 Symposium on VLSI Technology*, Honolulu, 2010, pp. 205-206.
[37] Y. Lei *et al*., “Enhanced read performance for phase change memory using a reference column,” *IEICE Electron. Expr.*, 2017, 14(5), pp. 1-10.
[38] G. Liu, et al. "Threshold switching in SiGeAsTeN chalcogenide glass prepared by As ion implantation into sputtered SiGeTeN film." *Applied Physics Letters* 111.25 (2017): 252102.
[39] Q. Wang *et al*., “Methods to speed up read operation in a 64Mbit phase change memory chip,” *IEICE Electron. Expr.*, 2015, 12(20), pp. 1-6.